VALIDATION OF CALTRANS ORDINARY BRIDGE MODELING APPROACH USING CSMIP DATA

Yijun Xiang, Jawad Fayaz, Farzin Zareian

Department of Civil & Environmental Engineering
University of California, Irvine

Abstract

This study aims at validating the modeling approaches of ordinary bridge structures suggested by Caltrans (SDC 2013; referred to as *SDC* models) and sophisticated models suggested by researchers, herein termed as *Stick* models. The validation is conducted using the CSMIP sensor data of four ordinary bridges in California with seat-type, and monolithic abutments. The backbone curves of the structural components of the *Stick* model including shear keys, abutment piles, and backfill soil are updated using Particle Swarm Optimization. This study yields the guidelines for calibration of parameters of bridge structural components and suggests improvements for modeling approaches of such bridges.

Introduction

Seat-type and monolithic box-girder bridges are among the most common types of highway bridges constructed in California. These bridges experienced different levels of damage such as rotation of decks, unseating of abutments, breakage of shear keys, and damage to columns during seismic events. As an essential part of public infrastructure, bridges are expected to be designed in a way that they survive and maintain functionality after major earthquake excitations. With this backdrop, advanced bridge modeling approaches along with nonlinear time-history analysis is needed to provide insight for the proper and safe design of bridge structures. There is a substantial body of research focusing on designing, modeling and nonlinear behavior of seat-type and monolithic bridges. Current bridge design specifications in California (Caltrans SDC, 2013) include seismic design criteria for Ordinary Standard bridges and their components including abutments, superstructure, substructure support systems and foundations. Caltrans SDC details how bridge design engineers should proportion bridge components, and conduct analyses to capture the bridge behavior at the component- and system-level during design level seismic excitations.

During the past decades, researchers have developed analytical models for bridge structures and investigated their behavior during seismic excitations. In particular, Mackie and Stojadinovic (2007) developed bridge structure design equations by considering uncertainty in the hazard, demand, damage, and loss to the bridge using performance-based methodologies. Kaviani et al. (2012) modeled reinforced concrete bridges with skewed-angled seat-type abutment; they concluded that bridges with large abutment skew angles bear a higher probability of collapse. Ramanathan et al. (2015) suggested finite element bridge modeling approaches for three types of bridges: straight, curved and skewed bridges. They compared analytical response with recorded sensor data and tested the fragility and seismic vulnerability among bridge

components for each bridge type. Choi (2002) investigated the nonlinear behavior and seismic capacity of monolithic bridges. By performing nonlinear static pushover analysis, they showed that the lateral displacement of monolithic bridge is reduced due to end-restraining effect of the abutment. Other researches have focused on the modeling of bridge components such as shear keys, abutments, elastomeric bearing, and backfill soil. Rollins and Jessee (2013) performed laboratory tests on abutment walls with several skew angles and developed an adjustment factor to account for the reduced capacity due to skew angles. Laboratory tests conducted by Kottari (2016) developed response curves of shear keys further improved the knowledge of modeling approaches of bridge structures. The recent modeling approach used by Fayaz et al. (2019) combines the latest literature on the bridge component models to develop a better representation of real bridges.

Since the goal of this study is to validate the bridge modeling approach by matching recorded data with analytical results from finite element models, engineering optimization approaches are utilized to estimate and evaluate the key bridge parameters of bridge components (e.g., yielding point of shear key, stiffness of abutment piles, stiffness of backfill soil). Although optimization methods are widely used in system identification and model updating of bridge and building structures (a list of previous research work is presented in the following), however, this study proposes an applied optimization method that is tailored for bridge structures with field data. Ebrahimian et al. (2017) updated a nonlinear finite element model of a frame-type structure by minimizing the discrepancies between predicted and measured response; their work, among others, are conducted using simulated data instead of recorded data. Nasrellah and Manohar (2011) proposed an identification method that uses particle filtering to capture the behavior of structures including both computational models and models from laboratory and field tests. Song and Dyke (2014) proposed a real-time dynamic model updating method to match a modified Bouc-Wen model using data from two shake table tests. Lagaros et al. (2002) investigated evolutionary algorithms including Genetic Algorithms and Evolution Strategies, and optimized the weight of two space structures with inter-story drift being the constraints. Yang and Soh (1997) used Genetic Algorithm with a tournament selection strategy for configuration optimization of truss structures with up to 112 members. Perez and Behdinan (2007) verified the effectiveness of Particle Swarm Optimization method on structural optimization tasks by estimating the cross-sectional area, allowable displacement, and stresses for members in a 25-bar truss system.

This research focuses on the validation of bridge modeling approaches, especially the parameters of the backbone curves of bridge components, by comparing the discrepancy between sensor recorded response and analytical response using two modeling approaches: *SDC* and *Stick* modeling approaches. *SDC* refers to the bridge modeling approach suggested in Seismic Design Criteria (SDC) (2013). The *Stick* modeling approach is presented in Fayaz et al. (2019) that is borrowed from a collection of bridge modeling approaches available in current literature. The difference in response data from these two models is analyzed, and the difference in the modeling of bridge components of these two modeling approaches are discussed. The *Stick* modeling approach is further updated using Particle Swarm Optimization to minimize the discrepancy between recorded and simulated response. This study assesses the appropriateness of the current *Stick* modeling approach and updates a better setting of key bridge parameters in terms of the match between analytical response using the modeling approach and the true recorded response.

Bridge Models

Finite Element models of the bridges were developed in *OpenSees* (McKenna et al., 2010). The finite element models are comprised of: abutments, shear keys, column bents, elastomeric bearing pads, backfill soil, and superstructure. An illustration of the model is provided in Figure 1 and Figure 2 for seat-type abutment bridges and monolithic abutment bridges, respectively. The models are based on the bridge models presented in Omrani et al. (2017); however, their structural component models are upgraded, and associated modeling parameters are updated (Fayaz et al., 2019).
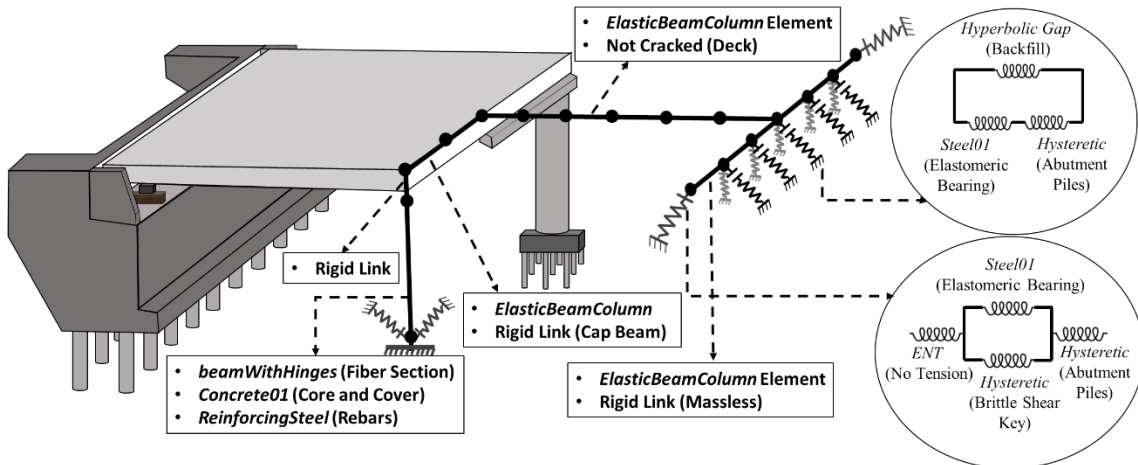
Figure 1: Illustration of the finite-element model of bridges with seat-type abutments
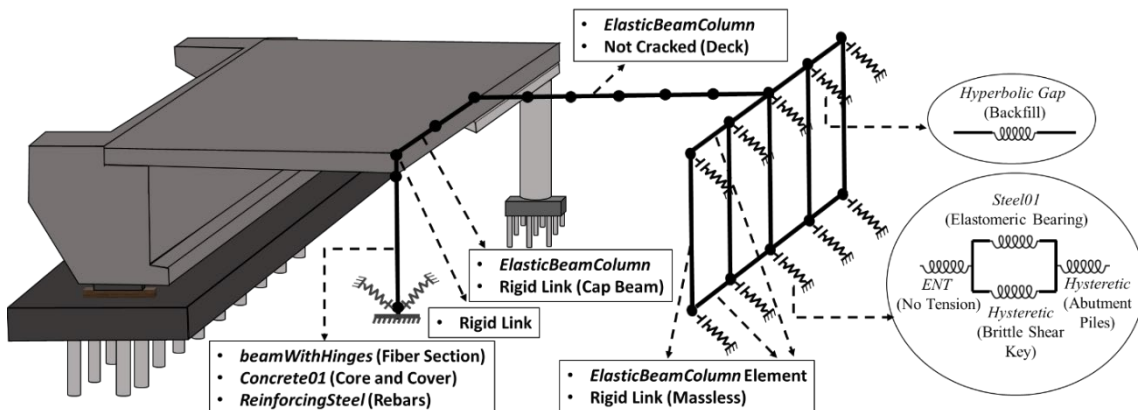
Figure 2: Illustration of the finite-element model of bridges with monolithic abutments

Caltrans SDC (2013) recommends the superstructure be designed to remain elastic during an event of Earthquake; therefore, the superstructure is modeled with `elasticBeamColumn` using uncracked section properties. To capture the dynamic response accurately, the mass of the superstructure is distributed throughout the length of the deck with each span's mass being distributed in ten intervals. The bridge columns are modeled using `beamWithHinges` element (two Gauss integration points) with fiber-discretized cross-sections to model confined concrete for the core, unconfined concrete for the cover and steel rebars. The nonlinear behavior of the columns is concentrated at two plastic hinges at the opposite ends connected by a linear elastic

element. The plastic hinge length is determined based on Caltrans SDC (2013). Assuming a monolithic construction of cap beam and columns, the cap beam is modeled as a rigid bent using `elasticBeamColumn` element with high torsional, in-plane, and out-of-plane stiffnesses. The concrete and steel are modeled using Concrete01 and `ReinforcingSteel` materials, respectively, which are available in *OpenSees*. The base of bridges is simulated as fixed and pinned connections for single-column bent and multiple-column bent, respectively, with the stiffness of connections arising from piles beneath. The piles under the bridge columns are modeled using elastic springs with the horizontal stiffnesses described as per Choi (2002).

Stick Modeling Approach

Shear keys are designed and modeled in a brittle/isolated manner using the `hysteretic` spring model available in *OpenSees*. The model is defined with a trilinear backbone curve as given in Figure 3d. The shear key is designed as per Caltrans SDC (2013) with area of vertical reinforcement (A_{vsk}) calculated as per Eq. 1, P_{dl}^{sup} is the superstructure dead load reaction at the abutment and f_{ye} is the yield strength of steel rebars. Based on past experimental observations detailed in Kottari (2016), the sliding shear resistance of an isolated shear key is associated with two states: i) shear resistance at first sliding (V_{slid}) and ii) ultimate sliding shear resistance (V_u) right before the rupture of the dowel bars. Assuming a smooth construction joint is provided, the shear resistance due to the dowel action (F_d) of the vertical dowel bars is calculated using Eq. 2 which leads to the calculation of V_{slid} in Eq. 6 through Eqs. 3, 4, and 5. Based on the equilibrium of the horizontal and vertical forces (Bozorgzadeh et al., 2006). V_u is calculated as per Eq. 7.

$$A_{vsk} = \frac{\alpha \times P_{dl}^{sup}}{1.8 \times f_{ye}} \quad ; \qquad 0.5 < \alpha < 1 \qquad \text{Eq. (1)}$$

$$F_d = \sum^{\# \, of \, Vertical \, bars} \sqrt{2.\,M_{pl,i}.\,f_{cb,i}.\,d_{b,i}} \qquad \text{Eq. (2)}$$

$$M_{pl,i} = \frac{f_y.\,d_{b,i}^{\,3}}{6} \qquad \text{Eq. (3)}$$

$$f_{b,i} = a_i.\,f_c^{\,1.2} \qquad \text{Eq. (4)}$$

$$a_i = 2.0 + \frac{0.5}{d_{b,i}} \qquad \text{Eq. (5)}$$

$$V_{slid} = \frac{T + F_d}{\left(1 - \mu_f.\,tan\beta\right)} \qquad \text{Eq. (6)}$$

$$V_u = \frac{\mu_f.\,cos\gamma + sin\gamma}{1 - \mu_f.\,tan\beta}.\,A_{vsk}.\,f_{su} \qquad \text{Eq. (7)}$$

In these equations, $M_{pl,i}$ is the plastic moment capacity of bar i, and the compressive strength of confined concrete, $f_{cb,i}$, f_c is the uniaxial concrete compressive strength, $d_{b,i}$ is the diameter of bar i, β is the angle of the inclined face of the shear key with respect to a vertical plane, T is the cohesive force, and μ_f is the coefficient of friction of the smooth construction

joint ($\mu_f = 0.36$) (Kottari, 2016). γ is the angle of inclination of the vertical dowel bar (Angle of Kink). It is assumed that bond breaker is applied on the construction joint, hence $T = 0$ in Eq. 6. The value of γ is obtained from Kottari (2016) through interpolation for the provided diameter of dowel bars. The initial stiffness (k_1) of the backbone curve is computed through the summation of shear and flexural responses of the concrete cantilever action of the shear key (Omrani et al., 2017), while the stiffness of hardening (k_2) and softening (k_3) branches are expressed as a percentage of k_1 (ranging from 0.5 % to 2.5% for various rebar diameters) that are interpolated according to Kottari (2016).

The model of abutment comprises i) abutment piles, ii) backfill soil, and iii) elastomeric bearing pads. Piles of the abutments are modeled through a trilinear `hysteretic` spring model in *OpenSees* with the backbone curve defined as per Choi (2002). The backbone is presented in Figure 3b. The backfill soil is modeled using the `HyperbolicGapMaterial` material with a Generalized Hyperbolic Force-Deformation (GHFD) backbone (Shamsabadi and Kapuskar, 2006). The backbone is presented in Figure 3c. Hence, the active resistance of the abutment is provided by the piles while the passive action includes resistance due to the piles and backfill soil. The parameters described by Ramanathan (2012) are used to model the elastomeric bearing pads using the `Steel01` material, as shown in Figure 3a. The longitudinal behavior of the abutment is modeled using five springs in parallel connected by a rigid link while the transverse behavior is modeled using one spring on both ends of the abutment.
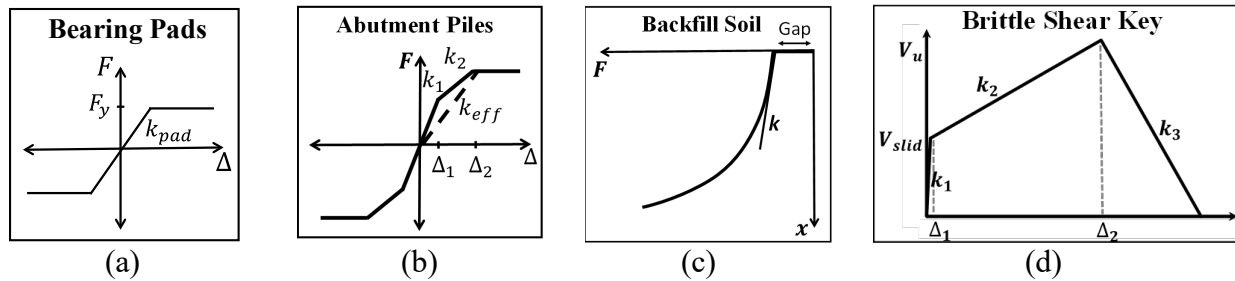

Figure 3: Details of the finite-element model of bridge structural components: a) Bearing pads response, b) Abutment pile response, c) Backfill soil response, and d) Shear key response

SDC Modeling Approach

Simplified analysis per Caltrans SDC (2013) requires the use of cracked flexural stiffness I_{eff} for ductile members. I_{eff} for reinforced concrete box girder sections are estimated between $0.5I_g$ to $0.75I_g$. This reduction factor is used for other superstructure types and cap beams. The torsional moment of inertia for columns is reduced to $0.2J_g$. Modeling of abutment longitudinal response is accomplished by a bilinear approximation of force-deformation relationship, including an effective abutment stiffness with expansion gaps considered for seat-type abutments and a realistic embankment fill response. The initial stiffness is proportional to the backwall/diaphragm height h, for seat-type and monolithic abutments, respectively, based on Eq. 8. In this equation, w is the projected width of backwall/diaphragm for seat-type and monolithic abutments, respectively. Eq. 9 yields the passive pressure force resisting the movement of the abutment, and Eq. 10 shows the effective abutment wall area for either seat-type or monolithic abutment type. For transverse abutment response, if the abutment is seat-type, a nominal transverse spring stiffness is taken as 50% of the elastic transverse stiffness of the adjacent bent.

While transverse stiffness of a monolithic type abutment is conservatively estimated as 40 kips/in per pile.

$$K_{abut} = \frac{50 kip/in}{ft} . w . \frac{h}{5.5ft} \qquad \text{Eq. (8)}$$

$$P = A_e . 5ksf . \frac{h}{5.5ft} \qquad \text{Eq. (9)}$$

$$A_e = h . w \qquad \text{Eq. (10)}$$

Bridge I

Bridge II

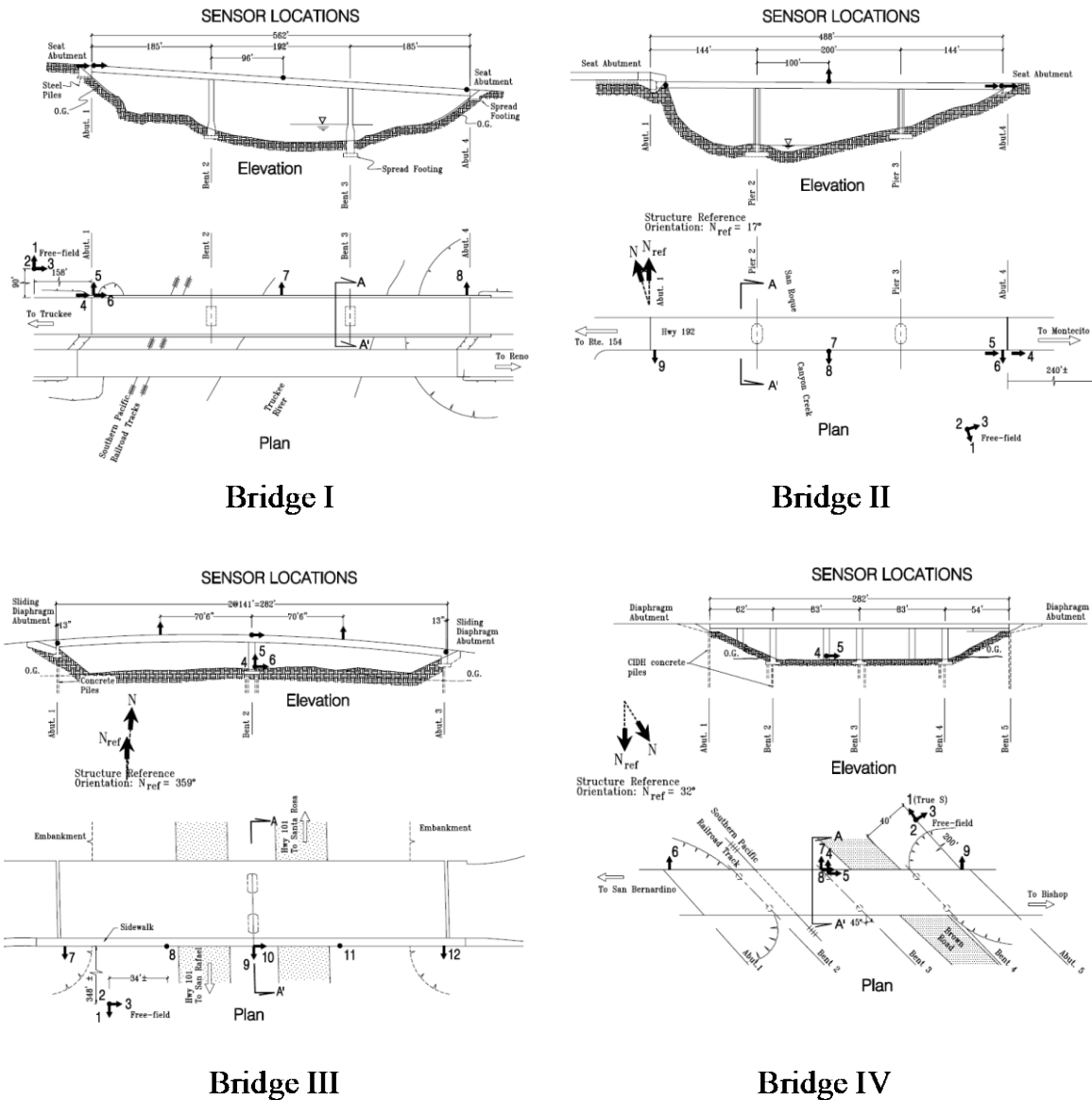
Bridge III

Bridge IV

Figure 4: Configurations of selected CSMIP instrumented bridges

Selected Bridges for Case Studies

Four CSMIP instrumented bridges are selected in this study: i) Truckee I-80 River Bridge, ii) Santa Barbara San Roque Canyon Bridge, iii) Rohnert Park Hwy 101 Bridge and iv) Ridgecrest-Hwy 395 Brown Road Bridge. Table 1 summarizes the basic information of the selected bridges, including the number of spans, the number of columns in each span, the skewness, and the abutment type. Figure 4 illustrates the configurations of bridge I, II, III and IV. Bridge I and II are selected to study the straight seat-type abutment bridges. Bridge III is a straight monolithic bridge, and bridge IV is a skewed-abutment monolithic bridge. All four bridges are modeled using both *Stick* and *SDC* modeling approaches (See Figure 1 and Figure 2) in *OpenSees* using the engineering drawings of the bridges. The key bridge components of bridge I and II include shear keys, backfill soil, abutment piles, elastomeric bearing pads, columns (with piles), and superstructure. Bridge III is modeled using foundational shear keys, backfill soil with the monolithic type abutment, abutment piles, elastomeric bearing pads, and columns (with piles). While bridge IV is modeled using backfill soil with the monolithic type abutment, abutment piles, and columns (with piles). Due to abutment skewness in bridge IV, the stiffness and force of backfill soil are reduced with reduction factors suggested by Rollins et al. (2013). The springs are altered as a function of the distance of the springs with respect to the center of the bridge (Kaviani et al. 2012) in the optimized *Stick* model.

Table 1. Selected bridges from CSMIP database

Bridge	I	II	III	IV
Name	Truckee I-80 River Bridge	Santa Barbara San Roque Canyon Bridge,	Rohnert Park Hwy 101 Bridge	Ridgecrest Hwy 395 Brown Road Bridge
Number of Spans	3	3	2	4
Column Bent	Single-column	Single-column	Two-column	Two-column
Skewness	Straight	Straight	Straight	Skewed
Abutment Type	Seat-type	Seat-type	Monolithic	Monolithic

Optimization Method

To obtain a better estimate of the key bridge parameters of the bridge components, Particle Swarm Optimization (PSO) is adopted in this study. The algorithm works by initializing a population of candidate particles, which move in the search space to minimize the objective function. Each particle will update itself based on its own local best-known position as well as the global best-known position found by the entire group. PSO is selected due to its convenience in implementation, the fewer number of hyperparameters, and the capability of dealing with high dimensional optimization problems. As a gradient-free algorithm, PSO does not require the objective function surface to be differentiable and is suitable in this study given that the objective function measures the discrepancy between recorded response and analytical response.

PSO Formula

As mentioned in Eq. 11, the velocity of particle i at dimension d at the kth step (i.e., v_{id}^k) is updated by three terms. The first term represents the velocity of particle i at the previous step

factored by w^k, where w (Eq. 13) decreases linearly as the algorithm carries on with index k (K is the total number of steps). The second term in Eq. 11 guides the particle's position (i.e., x_{id}^k) towards the local best position (i.e., x_{id}^{p-best}). The third term in Eq. 11 guides the particle towards the global best position (i.e., x_d^{g-best}), which is not a function of i. c_1 and c_2 are the hyperparameters that can be tuned as learning rates, and r_1 and r_2 are random variables ranging from 0 to 1 in order to increase uncertainty in the searching process. Finally, the position is updated by summing up the previous position and the velocity as shown in Eq. 12.

$$v_{id}^k = w^k v_{id}^{k-1} + c_1 r_1 \left(x_{id}^{p-best} - x_{id}^{k-1} \right) + c_2 r_2 \left(x_d^{g-best} - x_{id}^{k-1} \right) \qquad \text{Eq. (11)}$$

$$x_{id}^k = x_{id}^{k-1} + v_{id}^{k-1} \qquad \text{Eq. (12)}$$

$$w^k = w_{max} - (w_{max} - w_{min}) \frac{k}{K} \qquad \text{Eq. (13)}$$

The Objective Function and Updated Parameters

Several objective functions were implemented, tested, and critiqued. These objective functions were various combinations of the squared-sum-of-discrepancy between analytical response and recorded response. The discrepancies were measured in i) time history acceleration data, ii) acceleration data in the frequency domain using Fourier Transformation, iii) peak displacement value. The most representative objective function that maintains the signal signature was the one that measures the discrepancy in the time domain (see Eq. 14). The match in frequency domain leads to large errors due to the large fluctuation in frequency domain plus it will not include data seasonality that is evident in the time domain acceleration history of each bridge. The match in peak displacement compares only one data point and leads to an unrealistic estimation of parameters.

The measure of discrepancy between recorded acceleration response and simulated acceleration response in the time domain is shown in Eq. 14. The discrepancy is summed over all strong motion data points along time history and overall sensor locations where the recorded response is measured. Acceleration instead of displacement is picked as the response where the error is computed due to the rich information contained in acceleration data and its stationarity compared to displacement time history.

$$J(\boldsymbol{\theta}) = \sum_{j=1}^{N_{sen}} \sum_{l=1}^{\tau} \frac{[\ddot{u}_j(l\Delta t) - \ddot{\hat{u}}_j(l\Delta t)]^2}{\sum_{p=1}^{\tau} [\ddot{u}_j(p\Delta t)]^2} \qquad \text{Eq. (14)}$$

Objective functions are functions that vary with the change of the set of bridge parameters vector $\boldsymbol{\theta}$ ($\boldsymbol{\theta} = \{\theta_1, \cdots, \theta_d, \cdots, \theta_{D_B}\}$; $D_B \in \{D_I, D_{II}, D_{III}, D_{IV}\}$, see Table 2 for the definition of D_B). Given that the four selected bridges have different key bridge structure components, the selection of $\boldsymbol{\theta}$ and the optimization dimension also vary. Table 2 provides the key bridge parameters updated by the optimization method and the corresponding dimension

(number of parameters). The searching space is limited between $\theta_d/10$ and $10\theta_d$ for each dimension d, and a quadratic penalty is added to the objective function if constraints are violated.

Results and Discussion

The overall results of the match between recorded acceleration response and the simulated acceleration response imply the inappropriateness of the *SDC* modeling approach as well as the insufficiency in the *Stick* modeling approach. The performances of the modeling approaches vary with the type of bridges. The response from the models developed using the *SDC* modeling approach is closer to field data than the models based on the *Stick* modeling approach for seat-type abutment bridges; an opposite observation is made for monolithic abutment bridges. The results clearly show that the *SDC* modeling approach underestimates bridge stiffness in the longitudinal direction. The optimization method assists the *Stick* modeling approach, but the benefit of the optimization process is limited. That is because the dynamic properties of the bridge models highly depend on the model geometry and types of elements utilized (sufficiency of the analytical models).

Table 2. Bridge parameters updated using optimization method for four selected bridges

Bridge	Bridge parameters θ of key bridge structure components	Num. of Dim. (D_B)
I & II	Shear key sliding shear: V_{slid}, Deformation corresponding to Shear key sliding shear:u_1, Shear key ultimate shear: V_{usk}, Stiffness of backfill soil: K_{abut}, Force of backfill soil:f_{abut}, Stiffness of abutment piles: K_{eff}, Coefficient of friction for bearing pads: μ, Column moment of inertia: I_c, Damping Ratio: ξ	$D_I = D_{II} = 9$
III	Shear key sliding shear and corresponding deformation in transverse and longitudinal directions: V_{slid_T}, u_{1_T}, V_{slid_L}, u_{1_L}, Shear key ultimate shear in transverse and longitudinal directions: V_{usk_T}, V_{usk_L}, Stiffness and force of backfill soil: K_{abut}, f_{abut}, Stiffness of abutment piles: K_{eff}, Coefficient of friction for bearing pads: μ, Column moment of inertia: I_c, Damping Ratio: ξ	$D_{III} = 12$
IV	Backfill stiffness and force K_{abut}, f_{abut}, Stiffness of abutment piles: K_{eff}, Column moment of inertia I_c, Damping Ratio ξ	$D_{IV} = 5$

Seat-type Abutment Bridges

The performance of the two modeling approaches are investigated for Bridge I for illustration purposes; the same patterns and trends are found in Bridge II, whose results are omitted due to page limit. For simplicity, the results associated with the *SDC* and *Stick* modeling approaches are labeled as *SDC*, and *Stick*, respectively. The results associated with the optimized *Stick* modeling approach is labeled as *OptStick*. Figure 5 presents the response at the edge of the deck in the longitudinal direction, both in time domain and in frequency domain, for all three modeling approaches. In the frequency domain, *SDC* generates a spurious spike of frequency content near 1.8Hz, and this leads to the spurious low frequency waveform in time domain. *Stick*, applied with the same 5% damping ratio as *SDC*, captures the recorded waveform more accurately compared to *SDC*. This is mainly due to the inappropriateness of

longitudinal abutment modeling of *SDC*, where the longitudinal stiffness is unrealistically small. In this case, the improvement in performance from optimization method is very limited, as the response from *OptStick* and *Stick* are almost identical in longitudinal direction.
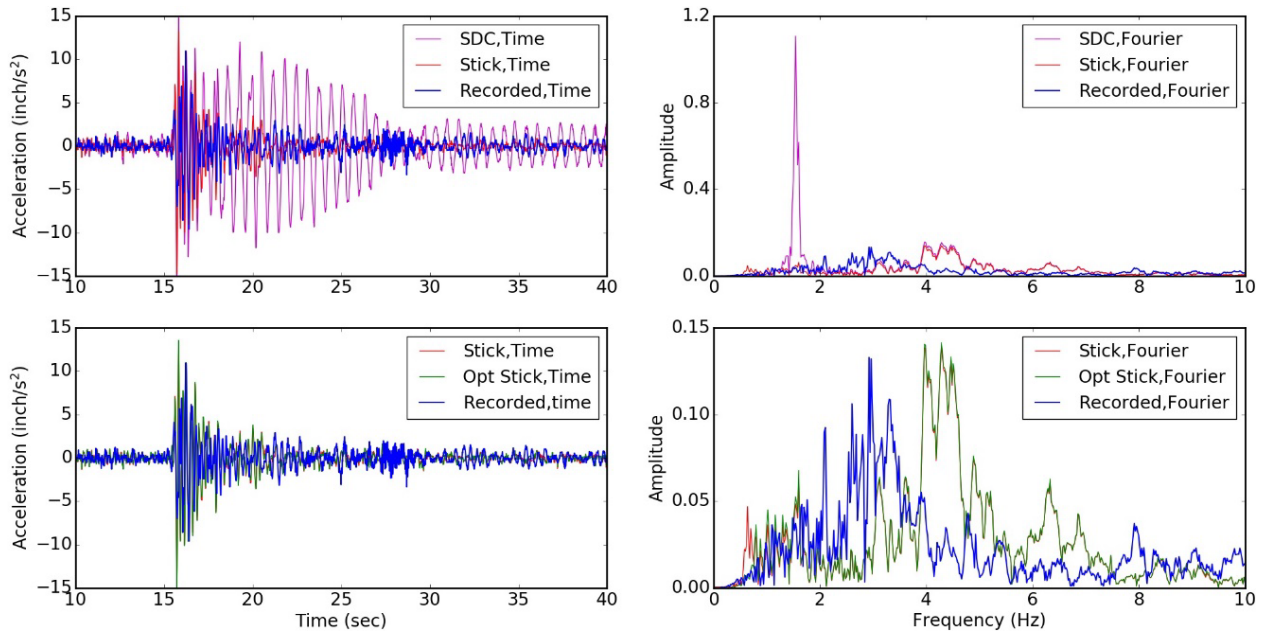

Figure 5: Deck response at the edge of Bridge I in longitudinal direction subject to Whitehawk Earthquake M_w = 4.7 occurred on Oct 26, 2011
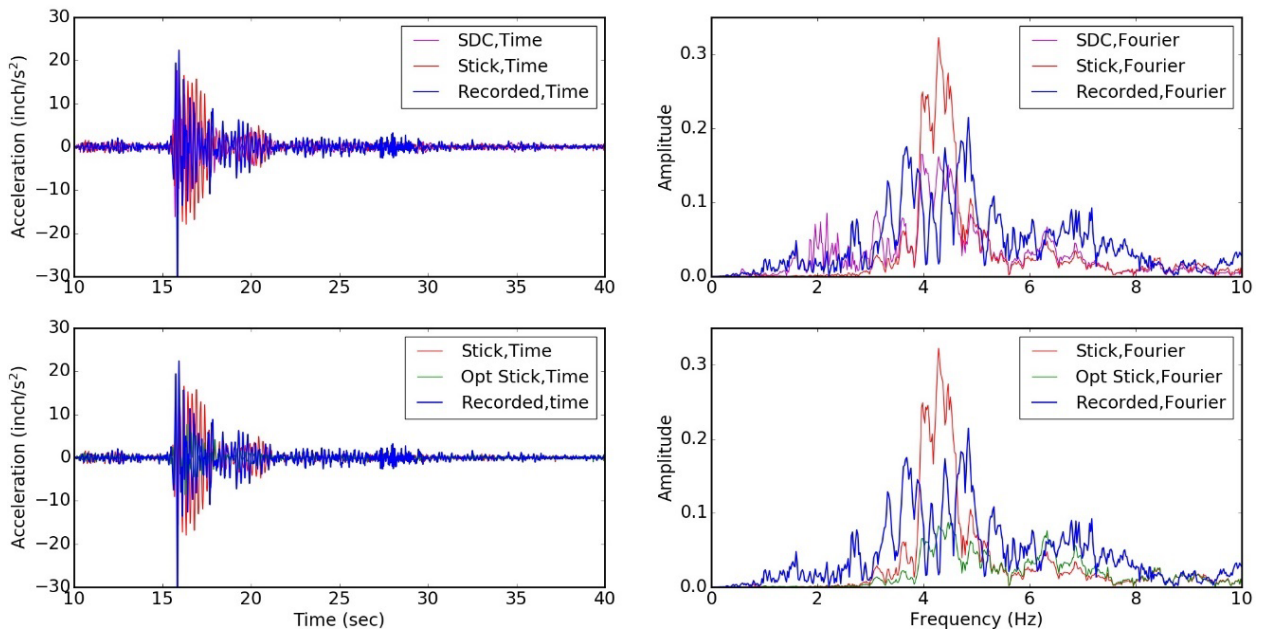

Figure 6: Deck response at the edge of Bridge I in transverse direction subjected to Whitehawk Earthquake M_w = 4.7 occurred on Oct 26, 2011
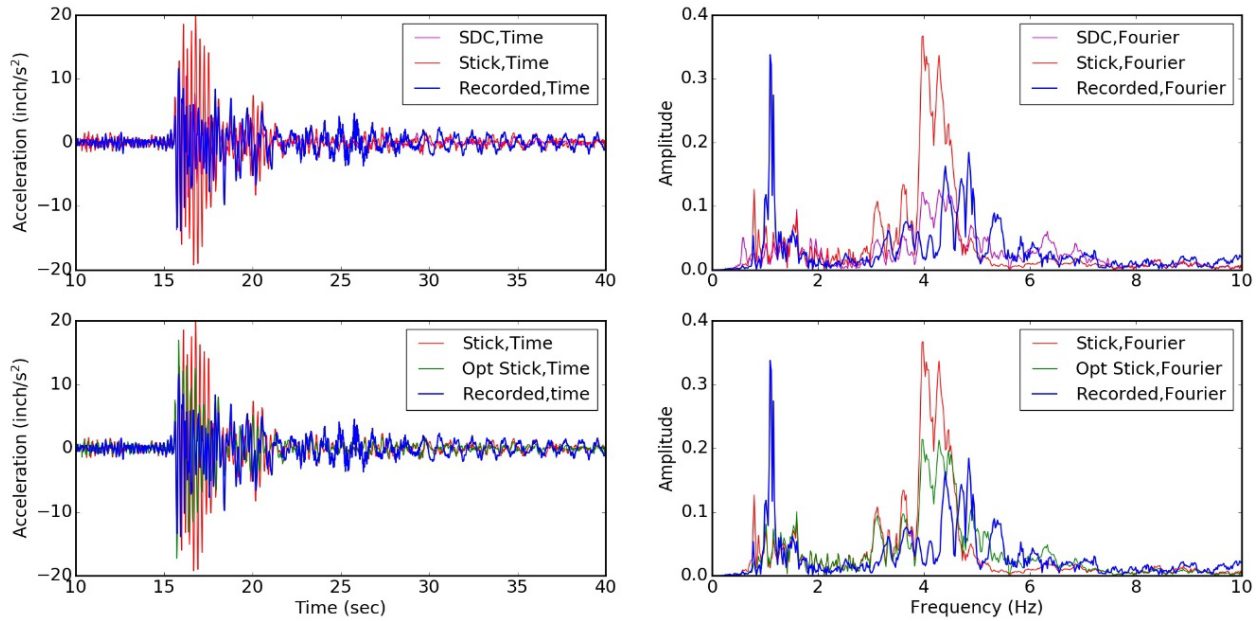
Figure 7: Deck response in the middle of Bridge I in transverse direction subject to Whitehawk Earthquake $M_w = 4.7$ occurred on Oct 26, 2011

Figure 6 shows the response of the edge of the deck in the transverse direction. In the frequency domain, all three modeling approaches are able to capture the main frequency content around 4Hz. Although the amplitude of the frequency content estimated from *Stick* is slightly higher than the recorded one, *OptStick* brings the amplitude in frequency domain down towards the recorded data, and this can be verified in the time domain as the higher amplitude in acceleration in *Stick* is reduced to the same level of the recorded data by *OptStick*. In this case, *SDC* successfully matches the recorded response in both time and frequency domain, which implies that *SDC* provides a relatively accurate modeling approach to capture the response at edge of the deck in the transverse direction.

Figure 7 shows the response in the middle of the deck in transverse direction. All three modeling approaches are able to capture the two main frequency contents at 1 Hz and 4 Hz. Although the amplitude of the first main frequency content (1 Hz) is underestimated by all three modeling approaches, and *Stick* overestimates the amplitude of the second main frequency content (4 Hz). Similar to the transverse response at the edge of the deck, *OptStick* helps in reducing the fictitious amplitudes generated by *Stick*, and this can be seen in both time domain and frequency domain results. *SDC* can still match the recorded response relatively well in the transverse direction.

Monolithic-type Abutment Bridges

Bridge IV is picked to demonstrate the difference in modeling approaches for monolithic bridges; the bridge was subjected to the Ridgecrest Earthquake that occurred on Jul 5, 2019, with $Mw = 7.1$. Figure 8 shows the abutment response in the transverse direction. In frequency domain, *Stick* and *Optstick* are both able to capture the frequency contents, and they both follow the trends of the recorded data, although there is a slight shift in *OptStick* around 2Hz, and the

estimated amplitude for that frequency content is much higher than the recorded amplitude. However, the performance of *SDC* is quite poor that it creates a fictitious frequency content around 1.8 Hz with a considerably large amplitude. This modeling inaccuracy can be confirmed in time domain, as *SDC* has a low-frequency waveform with higher amplitude. In this case, *Stick* performs slightly better than *SDC* in terms of amplitude estimation, while *OptStick* alleviates the overestimation of amplitude.

For the transverse response in the middle of the deck, as shown in Figure 8, while *SDC* has the same inaccurate estimate of the main frequency content, *Stick* and even *OptStick* are not able to capture the true frequency, which is around 3 Hz. In time domain, *SDC*, as expected, displays a low-frequency high-amplitude waveform, while *Stick* can match the recorded time history trend much more precisely. *OptStick* further updates *Stick* and make the fitting of response much closer to the recorded data.

Parameters of Three Modeling Approaches

Tables 3-5 summarized the key bridge parameters used in *SDC* and the key bridge parameters used in *Stick* and updated in *OptStick* for both seat-type and monolithic abutment bridges. Each bridge is tested with two ground motions, so that there are three sets of estimated parameter values: parameters of the original *Stick*, parameters updated using GM1 and parameters updated with GM2.
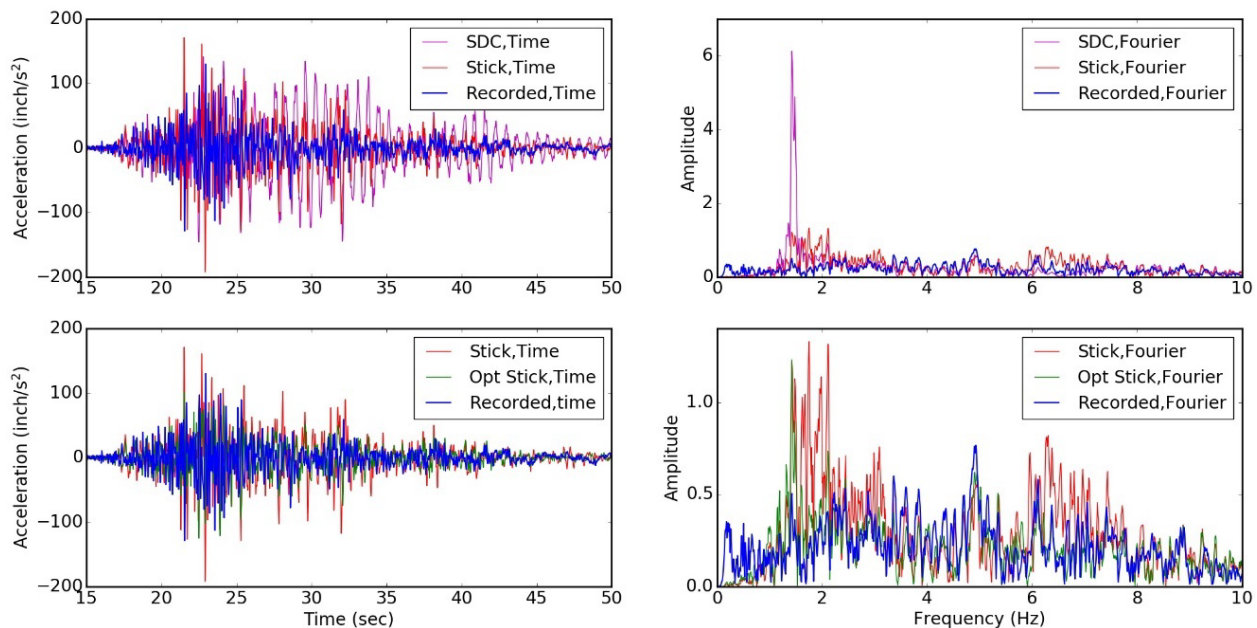

Figure 8: Abutment response of Bridge IV in transverse direction subject to Ridgecrest Earthquake $M_w = 7.1$ occurred on Jul 5, 2019
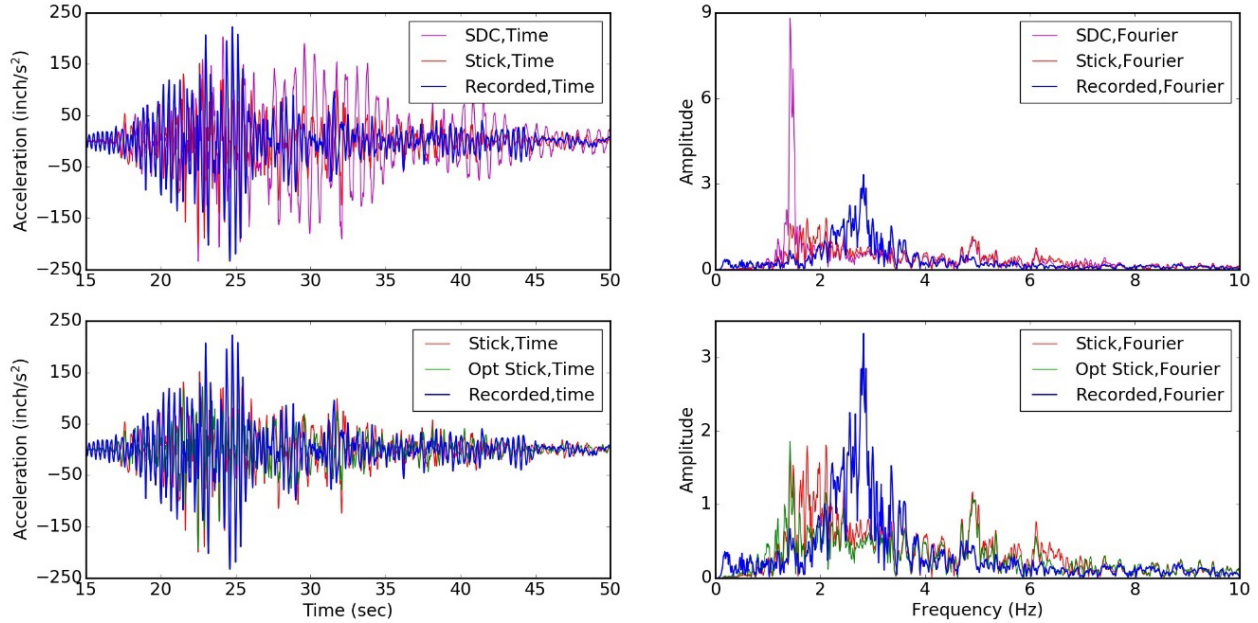
Figure 9: Deck response in the middle of Bridge IV in transverse direction subject to Ridgecrest Earthquake M_w = 7.1occurred on Jul 5, 2019

Table 3. Bridge parameters used in *SDC* modeling approach

Bridge	I	II	III	IV
Abutment longitudinal stiffness K_{eff}(kips/in)	1675	1632	6854	1761
Backfill Passive Pressure Force P_{bw}(kips)	2763	2938	8910	1673
Transverse Spring Stiffness (kips/in)	242	1621	480	280
I_{col}(in^4)	23×10^6	34×10^6	2×10^6	4×10^5
J_{col}(in^4)	47×10^6	67×10^6	4×10^6	8×10^5
I_{deck} (in^4)	40×10^7	50×10^7	107×10^7	28×10^7
Damping Ratio ξ	0.05	0.05	0.05	0.05

Table 4. Seat-type bridge parameters in *Stick* modeling approach

Bridge	I			II		
Model	*Stick*	*OptStick*GM1	*OptStick*GM2	*Stick*	*OptStick*GM1	*OptStick*GM2
V_{slid}(kips)	249	132	158	158	246	272
V_{usk}(kips)	1055	959	1484	715	1423	1065
u_1(in)	0.006	0.004	0.002	0.007	0.004	0.008
K_{abut}(kips/in)	593	388	430	662	287	260
f_{abut}(kips)	291	340	225	366	502	271
K_{eff}(kips)	2000	3346	2842	1680	687	655
μ	0.189	0.042	0.112	0.192	0.495	0.551
I_c(in^4)	23×10^6	17×10^6	22×10^6	34×10^6	17×10^6	13×10^6
ξ	0.05	0.16	0.13	0.05	0.19	0.17

Table 5. Monolithic bridge parameters in *Stick* modeling approach

Bridge	III			IV		
Model	*Stick*	*OptStick*[GM1]	*OptStick*[GM2]	*Stick*	*OptStick*[GM1]	*OptStick*[GM2]
$V_{slid\,T}$(kips)	178	150	208			
$V_{usk\,T}$(kips)	904	1393	718	No Transverse Shear Key		
$u_{1\,T}$ (in)	0.03	0.07	0.04			
K_{abut}(kips/in)	876	1191	908	221	331	292
f_{abut}(kips)	700	322	470	129	163	48
K_{eff}(kips)	480	485	267	280	211	134
μ	0.148	0.343	0.378	No Bearing Pad		
I_c(in^4)	20×10^5	22×10^5	14×10^5	4×10^5	2×10^5	2×10^5
ξ	0.05	0.18	0.18	0.05	0.16	0.17
$V_{slid\,L}$(kips)	357	388	271			
$u_{1\,L}$(in)	0.014	0.002	0.01	No Longitudinal Shear Key		
$V_{usk\,L}$(kips)	1809	2250	1057			

Conclusion

Bridge modeling approaches are essentially important as they give guidance for the design and retrofit of bridge structures. This study investigated three bridge modeling approaches; namely, *SDC*, *Stick,* and *OptStick*, using four CSMIP instrumented bridge structures including: Truckee I-80 River Bridge, Santa Barbara San Roque Canyon Bridge, Rohnert Park Hwy 101 Bridge and Ridgecrest Hwy 395 Brown Road Bridge. The first two are seat-type abutment bridges, and the last two are monolithic abutment bridges.

SDC uses the simplified modeling approach per Caltrans SDC (2013) for the longitudinal and transverse abutment, as well as columns and structure by using cracked section properties. *Stick* combines backbone models of shear keys, abutment piles, elastomeric bearing pads, and backfill soil to represent a better configuration of bridge structures. *OptStick* stands for an optimized version of *Stick* via optimization techniques and updates the key bridge parameters of bridge components in *Stick.* Acceleration response generated from these three modeling approaches is compared with the recorded response obtained from the CSMIP database. Time history data is also transferred into frequency domain using Fourier transformation in order to have a better understanding of the different performances from different modeling approaches.

For bridges with seat-type abutments, the *SDC* model was superior to other modeling types, especially in capturing the transverse response at the middle and the edge of the deck. *SDC* is able to capture the main frequency content of recorded response, and *SDC* response is closer to the recorded response compared to the more sophisticated *Stick*. However, seismic response is inaccurately estimated using the *SDC* model in the longitudinal direction. This is due to the modeling requirements that lead to a low abutment longitudinal stiffness in the *SDC* model. Although *Stick* sometimes leads to more inaccurate dynamic response, optimization methods help correct those discrepancies by updating the key bridge parameters, and the results from *OptStick* can be as precise as those from the *SDC*.

For monolithic bridges, the response from *Stick* has a better match with recorded response compared to the *SDC* model. *SDC* models often estimate spurious frequency contents, and the amplitude estimation in both time and frequency domains could be very different from that of a recorded response. Although *Stick* has a slight overestimation in amplitudes, it can capture the trends of recorded response. *OptStick* is able to reduce the fictitious amplitude estimation from a *Stick* so that the predicted response can be much closer to the recorded response in both time and frequency domains.

However, given the best updated results, it can be argued that even *OptStick* cannot capture every component of a real bridge structure accurately. This implies that the underlying and fundamental modeling assumptions of all models (i.e., *Stick* and *SDC*) require a re-evaluation, and a new modeling approach is required that can sufficiently and efficiently estimate bridge response during seismic excitations.

Acknowledgments

Reference

Bozorgzadeh, A., Megally S., Restrpo J., Ashford S.A. (2006), Capacity Evaluation of Exterior Sacrificial Shear Keys of Bridge Abutments. Journal of Bridge Engineering, **11**, 555-565.

Caltrans SDC (2013), Seismic Design Criteria. Version 1.7, California Department of Transportation, Sacramento, CA.

Choi, E. (2002), Seismic analysis and retrofit of mid-America bridges. Ph.D. Thesis, Department of Civil and Environmental Engineering, Georgia Institute of Technology, Atlanta (GA).

Ebrahimian, H., Astroza, R., Conte, J.P., de Callafon, R.A.(2017), Nonlinear Finite Element Model Updating for Damage Identification of Civil Structures using Batch Bayesian Estimation. *Mechanical Systems and Signal Processing* **84**, 194-222.

Fayaz, J, Xiang, Y., and Zareian, F. (2019), Performance Assessment of Bridges Under A Sequence of Seismic Excitations. *Computational Methods in Structural Dynamics & Earthquake Engineering* (*COMPDYN 2019*), Crete Island, Greece, June 2019

Kaviani, P., Zareian, F., Taciroglu, E. (2012), Seismic Behavior of Reinforced Concrete Bridges with Skew-anges Seat-type Abutments. *Engineering Structures* **45**, 137–150.

Kottari, A. (2016), Design and Capacity Assessment of External Shear keys in Bridge Abutments. Ph.D. Thesis, Department of Structural Engineering, University of California, San Diego, CA.

Lagaros, N.D., Papadrakakis, M., Kokossalakis, G. (2002), Structural Optimization using Evolutionary Algorithms. *Computers and Structures*, **80**, 571-589.

Mackie, K.R., Stojadinovic, B. (2007), Performance-based Seismic Bridge Design for Damage and Loss Limit States. *Earthquake Engineering and Structure Dynamics*, **36**,1953-1971.

McKenna, F., Scott, M. H., and Fenves, G. L. (2010), Nonlinear Finite Element Analysis Software Architecture using Object Composition. *Journal of Computing in Civil Engineering*, **24**(3), 95-107.

Nasrellah, H.A., Manohar, C.S. (2011), Finite Element Method Based Monte Carlo Filters for Structural System Identification. *Probabilistic Engineering Mechanics*, **26**, 294-307.

Omrani, R., Mobasher B., Sheikhakbari, S., Zareian, F., Taciroglu, E. (2017), Variability in the Predicted Seismic Performance of a Typical Seat Type California Bridge due to Epistemic Uncertainties in its Abutment Backfill and Shear-key Models. *Engineering Structures* **148**, 718–738.

Perez, R.E., Behdinan, K. (2007), Particle Swarm Approach for Structural Design Optimization. *Computers and Structures*, **85**, 1579-1588.

Ramanathan, K. (2012), Next generation seismic fragility curves for California bridges incorporating the evolution in Seismic design philosophy. Ph.D. Thesis, Department of Civil and Environmental Engineering, Georgia Institute of Technology, Atlanta (GA).

Ramanathan, K., Jeon, J., Zakeri, B., DesRoches, R., Padgett, J. (2015), Seismic Response Prediction and Modeling Considerations for Curved and Skewed Concrete Box-girder Bridges. Earthquake and Structures, **9**, 1153-1179.

Rollins, K., Jessee, S.J. (2013), Passive Force-Deflection Curves for Skewed Abutments. *Journal of Bridge Engineering* **18**, 1086-1094.

Shamsabadi, A, Kapuskar, M. (2006), Nonlinear Seismic Soil-abutment-structure Interaction Analysis of Skewed Bridges. In: *Proc 5th National Seismic conference on bridges and highways*, San Francisco, CA.

Song, W., Dyke, S. (2014), Real-time Dynamic Model Updating of a Hysteretic Structural System. Journal of Structural Engineering, **140**(3), 04013082.

Yang, J, Soh, C.K. (1997), Structural Optimization by Genetic Algorithms with Tournament Selection. *Journal of Computing in Civil Engineering*. **11**(3), 195-200.